Bulgarian Journal of Physics vol. **47** (2020) 32–42

Systematic Study of Multifragmentation in Au-Au Collisions

Supriya Goyal

Department of Physics, GSSDGS Khalsa College, Patiala-147001

Received *19 December 2019*

Abstract. We performed a systematic study of the formation of fragments with different mass ranges in ^{197}Au+^{197}Au collisions at incident energies between 20–1000 MeV/nucleon and at impact parameter between $\hat{b} = 0$–0.98. The aim of present study is to understand the complex dependence of fragment production on incident energy and impact parameter. Our results clearly indicate that the QMD simulations of ^{197}Au+^{197}Au predict different behavior for different mass ranges than for IMF's with a change in incident energy and impact parameter. All charge yields ($3 \leq Z_{\rm frag} \leq 12$) can be parameterized by a power law ($\propto Z_{\rm frag}^{-\varsigma}$) and no signal of liquid-gas phase transition is seen as no unique dependence of ς on impact parameter is seen.

KEY WORDS: Au+Au reaction, charge yields, heavy-ion collisions, quantum molecular dynamics (QMD) model.

1 Introduction

Various phenomena such as incomplete (and complete) fusion-fission at low incident energies as well as multifragmentation or a complete disassembly of the nuclear matter, are the typical characteristics seen in a heavy-ion reaction. Among these phenomena, multifragmentation is most common observable, which is obtained over wider range of the spectra e.g. in the light ion induced reactions at relativistic incident energies (in the GeV range) and in heavy-ion collisions between 20 and 1000 MeV/nucleon depending on the centrality of the reaction. Lot of experimental and theoretical studies are reported in the literature during last two decades on the breaking of colliding nuclei into pieces of different sizes. The last gem is still far from being fully understood since many studies are scattered and no systematic study is available. Ogilvie *et al.* [1], from ALADIN group, studied the emission of fragments in the reactions of ^{197}Au+^{12}C, ^{27}Al, ^{63}Cu at 600 MeV/nucleon. A 'rise and fall' in the multiplicity of intermediate mass fragments (IMF's), originating from the projectile was reported. Same trend of rise and fall was later on reproduced at incident energies of 250, 400 and 1000 MeV/nucleon [2, 3]. This rise and fall was reported to halt at an incident energy of 100 MeV/nucleon, where monotonic decrease was reported

with impact parameter [2]. In a similar attempt, ^{197}Au+^{197}Au reaction was analyzed for incident energies between 70 and 130 MeV/nucleon [4]. If one couples all these studies, it is evident that maximum production of IMF's is observed around 100 MeV/nucleon and there is a gradual decrease on both sides of it [2–5]. Since IMF's cannot survive in a violent reaction, therefore, the above peak in the rise and fall of fragments was found to be shifted towards peripheral geometries with increase in the incident energies [2, 3, 6].

In peripheral reactions at higher incident energies, multi fragment decays are also observed through the de-excitation of the spectator matter formed during the initial stages of the reaction [7]. Some, isolated experimental studies are also reported on the mechanism of fragment production and their associated properties by FOPI and INDRA groups [8]. Various scaling law for the cluster yields, ranking in the average size of the fragments and fluctuations in the cluster size as well as kinetic observables are also reported [9]. The EOS collaboration did measure the universality in the fragment inclusive yield for the reactions of ^{197}Au+^{197}Au between incident energies of 250 and 1150 MeV/nucleon. The suppression in the IMF multiplicity with increase in the beam energies for central collisions and its almost energy independent behavior for peripheral collisions was reported in the literature [10].

On the other side of the incident energy i.e., low energy regime, the distribution of the fragments produced in the events involving multifragmentation of excited sources was reported for the peripheral collisions of ^{197}Au+^{197}Au at 35 MeV/nucleon [11].

At the theoretical front, lots of isolated studies are available in the literature that explain the above experimental results on the fragment production, universal and 'rise and fall' behavior of IMF's, fragment correlations etc [12]. No study, however, is available under one umbrella, that gives us a view of the reaction dynamics and associated phenomena collectively. The present aim of this study, therefore, is at least two folds:

(i) To present a systematic study of the multifragmentation for the reaction of ^{197}Au+^{197}Au over entire incident energy and impact parameter range. This is with the view that no complete systematic studies are available in the literature for the reaction of ^{197}Au+^{197}Au. Earlier, ^{40}Ca+^{40}Ca reaction was studied [13]. Since ^{197}Au is very heavy nuclei, therefore, surface effects will be minimized in this case. We plan to see whether experimental measured trends are reproduced and whether we obtain certain peculiar behavior that may need immediate attention of experimentalists;

(ii) It has also found in the literature that excited nuclear matter will pass through a liquid-gas phase transition stage at some incident energy and if the fragments are formed at this stage, these may show some characteristics of the liquid-gas phase transition [14].

In one of the investigations of high-energy hadron-nucleus collisions revealed a power-law behavior of the inclusive mass distributions [15] similar to 'Fisher Droplet Model' analysis that have been applied to extract critical parameters and is found to be very close to those observed for liquid-gas phase transitions in macroscopic systems [16]. Consistent with this macroscopic analogy, values of critical parameter have been extracted from the analysis of charge/mass distributions [17], which suggests a critical behavior for $2 \leq \varsigma \leq 3$. Interestingly, some studies advocated a minimum in ς with variation in incident energy [18], whereas others just denied it [10]. Even, an accident occurrence of power law behavior in multifragmentation was also seen in some theoretical studies. The power law dependence in terms of impact parameter has also been performed in literature [1, 3, 7, 18, 19]. The systematic study done in the first part will be extended to also analyze the power law behavior and to correlate it with earlier scattered studies. For present study, we generate phase space using the quantum molecular dynamics (QMD) model [20,21] which is explained in Section 2. Results and discussion are explained in Section 3 and finally we summarizes the results in Section 4.

2 The Quantum Molecular Dynamics Model

The quantum molecular dynamics model [20, 21] simulates the reaction on an event by event basis. Here each nucleon i is represented by a Gaussian wave packet with a width of $\sqrt{L}$ centered around the mean position $\vec{r}_i(t)$ and mean momentum $\vec{p}_i(t)$. Here each nucleon is represented by a coherent state of the form

$$\phi_i(\vec{r},\vec{p},t) = \frac{1}{(2\pi L)^{3/4}} e^{\left[-\{\vec{r}-\vec{r}_i(t)\}^2/4L\right]} e^{[i\vec{p}_i(t)\cdot\vec{r}/\hbar]}. \tag{1}$$

The Wigner distribution of a system with $A_T + A_P$ nucleons is given by

$$f(\vec{r},\vec{p},t) = \sum_{i=1}^{A_T+A_P} \frac{1}{(\pi\hbar)^3} e^{\left[-\{\vec{r}-\vec{r}_i(t)\}^2/2L\right]} e^{\left[-\{\vec{p}-\vec{p}_i(t)\}^2 2L/\hbar^2\right]'}, \tag{2}$$

with $L = 1.08$ fm^2.

The center of each Gaussian (in the coordinate and momentum space) is chosen by the Monte Carlo procedure. The momentum of nucleons (in each nucleus) is chosen between zero and local Fermi momentum [$= \sqrt{2m_i V_i(\vec{r})}$; $V_i(\vec{r})$ is the potential energy of nucleon i]. Naturally, one has to take care that the nuclei, thus generated, have right binding energy and proper root mean square radii.

The centroid of each wave packet is propagated using the classical equations of motion

$$\frac{d\vec{r}_i}{dt} = \frac{dH}{d\vec{p}_i} \,, \tag{3}$$

$$\frac{d\vec{p}_i}{dt} = -\frac{dH}{d\vec{r}_i} \,, \tag{4}$$

where the Hamiltonian is given by

$$H = \sum_i \frac{\vec{p}_i^{\,2}}{2m_i} + V^{\rm tot} \,. \tag{5}$$

The total interaction potential $V^{\rm tot}$ reads as

$$V^{\rm tot} = V^{\rm Loc} + V^{\rm Yuk} + V^{\rm Coul} \,, \tag{6}$$

with

$$V^{\rm Loc} = t_1\delta(\vec{r}_i - \vec{r}_j) + t_2\delta(\vec{r}_i - \vec{r}_j)\delta(\vec{r}_i - \vec{r}_k) \,, \tag{7}$$

$$V^{\rm Yuk} = t_3 e^{-|\vec{r}_i - \vec{r}_j|/m} / \left(|\vec{r}_i - \vec{r}_j|/m\right) \,, \tag{8}$$

with $m = 1.5$ fm and $t_3 = -6.66$ MeV.

The static (local) Skyrme interaction can further be parametrized as:

$$U^{\rm Loc} = \alpha \left(\frac{\rho}{\rho_o}\right) + \beta \left(\frac{\rho}{\rho_o}\right)^{\gamma} . \tag{9}$$

Here α, β and γ are the parameters that define equation of state. The set of parameters corresponding to different equations of state can be found in Ref. [20].

3 Results and Discussion

For the present study, we simulated the reactions of ^{197}Au+^{197}Au between 20 and 1000 MeV/nucleon over entire collision geometry using soft equation of state along with energy dependent nucleon-nucleon cross-section. The calculations are performed using minimum spanning tree algorithm with microscopic binding energy cut (MSTB(2.1)) [21]. The freeze-out time is taken to be between 300–500 fm/c. For the low incident energies, such as 20 MeV/nucleon it is 500 fm/c, while for higher incident energies it is 300 fm/c.

In Figure 1, we display the final stage spectator [Figure 1(a)] and participant [Figure 1(b)] matter as well as anisotropic ratio $\langle R_a \rangle$ [Figure 1(c)], as a function of scaled impact parameter ($\hat{b} = b/b_{\rm max}$; where $b_{\rm max} = R_1 + R_2$; R_i is the radius of projectile or target) for various incident energies. We define nucleons with at least one collision as participant whereas all nucleons which do not suffer any collision are termed as spectator. The anisotropy ratio $\langle R_a \rangle$ is defined as

$$\langle R_a \rangle = \frac{\sqrt{\langle p_x^2 \rangle} + \sqrt{\langle p_y^2 \rangle}}{2\sqrt{\langle p_z^2 \rangle}} \,. \tag{10}$$

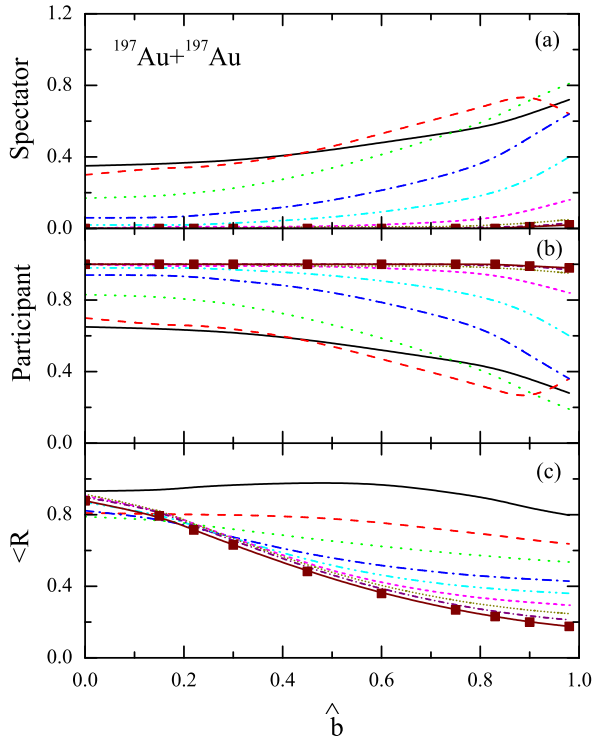

Figure 1. (Color online) The final stage spectators (a), participants (b), and anisotropy ratio $< R_a >$ (c) as a function of scaled impact parameter. The results obtained at 20, 40, 60, 100, 150, 250, 400, 600, and 1000 MeV/nucleon are displayed with solid, dashed, dotted, dashed-dotted, dashed-dotted-dotted, short-dashed, short-dotted, short-dashed-dotted lines, and solid squares, respectively.

Here p_x, p_y, and p_z are three components of momentum of the system. This anisotropy ratio $\langle R_a \rangle$ is an indicator of the global equilibrium of the system as it does not depend on the local density. The full global equilibrium average over large number of events will corresponds to $\langle R_a \rangle = 1$. From the figure, we see that the variation of the impact parameter leads to drastic change in the spectator/participant matter up to 400 MeV/nucleon, whereas beyond 400 MeV/nucleon, nearly impact parameter independent results can be seen. This happens due to the fact that the number of nucleon-nucleon collisions increases with the incident energy. From the values of $\langle R_a \rangle$, one can see that thermalization is better achieved in central collisions compared to peripheral ones. This is due to the decrease in the nucleon-nucleon collisions with increase in the impact parameter. Moreover, for central collisions, the variation in $\langle R_a \rangle$ with incident energy is less compared to peripheral collisions. With increase in the incident energy, the value of $\langle R_a \rangle$ decreases and this decrease is more pro-

nounced for peripheral collisions. This decrease points towards the increase of the transparency in nuclear matter with incident energy. The $\langle R_a \rangle$ saturates at lower incident energies for central collisions compared to peripheral ones. One should also note that, at all colliding geometries, $\langle R_a \rangle$ is almost independent of the incident energy beyond 400 MeV/nucleon.

In Figure 2, we display the final stage multiplicities of $\langle A^{\max} \rangle$ [Figure 2(a)], free nucleons [Figure 2(b)], fragments with mass $A = 2$ [Figure 2(c)], light charged particles (LCP's) ($2 \leq A \leq 4$) [Figure 2(d)], fragments with masses $A = 4$ [Figure 2(e)], $5 \leq A \leq 9$ [Figure 2(f)], $5 \leq A \leq 20$ [Figure 2(g)], intermediate mass fragments (IMF's) ($5 \leq A \leq 65$) [Figure 2(h)], and heavy mass fragments (HMF's) ($21 \leq A \leq 65$) [Figure 2(i)] as a function of scaled impact parameter. The idea of showing several different mass windows is to identify the different phenomenon that may appear in one mass window but not in other mass ranges. The size of heaviest fragment ($\langle A^{\max} \rangle$) will give us the possibility to look for partial fusion (if any) in the reaction of ^{197}Au+^{197}Au, whereas the emission of the free nucleons will show the disassembly (and hence vaporization) of the colliding matter. At low incident energies, very few nucleons are emitted from the excited compound matter which is followed by the emission of free nucleons and light fragments.

The heaviest fragment ($\langle A^{\max} \rangle$) yields several interesting points:

(i) One clearly sees that no partial fusion is seen in ^{197}Au+^{197}Au collisions even at low incident energies for all colliding geometries;

(ii) We also see that $\langle A^{\max} \rangle$ at low energies is nearly independent of the impact parameter. This is due to the fact that at low incident energies, the available phase-space is too small to allow the frequent nucleon-nucleon collisions. But at high incident energies, the dynamics is dominated by the frequent nucleon-nucleon collisions that depend strongly on the impact parameter, therefore, stronger impact parameter dependence is observed for $\langle A^{\max} \rangle$ at higher incident energies;

(iii) One also sees that $\langle A^{\max} \rangle$ is nearly independent of incident energy at peripheral collisions.

The emission of free nucleons exhibit just the opposite behavior to that of $\langle A^{\max} \rangle$. We notice a gradual increase in the emission of free nucleons with incident energy for central and semi-central collisions. If we label the phenomenon with $\approx 60\%$ matter as emitted nucleons as vaporization then we see the vaporization for central collisions above 150 MeV/nucleon.

The fragments with mass $A = 2$ and the LCP's, at central and semi-central collisions has a peak around 250 MeV/nucleon. The peak vanishes for peripheral collisions in all cases.

One should note that at low incident energies, the role of impact parameter vanishes in the multiplicity of fragments in all mass ranges. The rise and fall behavior in the multiplicity of fragments with $A = 4$, $5 \leq A \leq 9$, $5 \leq A \leq 20$,

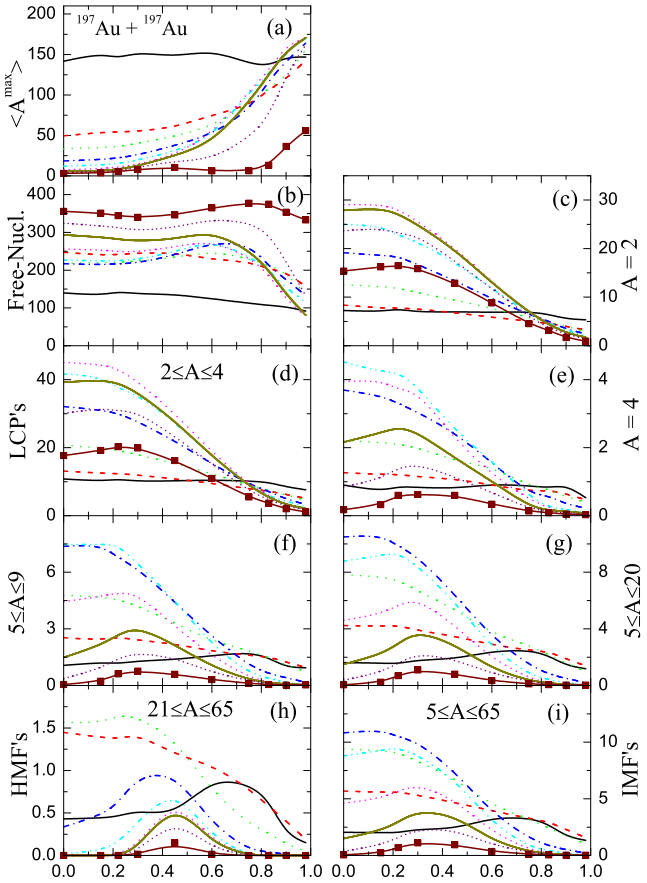

Figure 2. (Color online) Different fragment multiplicities as a function of the scaled impact parameter $\hat{b} = b/b_{\rm max}$. Lines and symbols are defined in Figure 1.

IMF's, and HMF's with scaled impact parameter is seen. We notice that:

(i) for central collisions ($\hat{b}$ = 0-0.15), there is a rise and fall in the fragment production with increase in the incident energy. The peak in the fragment production occurs at 150, 150, 100, 100, and 60 MeV/nucleon for fragments with $A = 4$, $5 \leq A \leq 9$, $5 \leq A \leq 20$, IMF's, and HMF's, respectively;

(ii) The fragments with mass $A = 4$, $5 \leq A \leq 9$, $5 \leq A \leq 20$, IMF's, and HMF's show a rise and fall for energies > 400, 250, 250, 150, and 100 MeV/nucleon, respectively.

It is clear from the values, that their is a gradual shift in the incident energy at which the peak occurs for different fragment ranges. While keeping the impact

parameter fixed, one needs higher incident energies to break the excited system into light fragments as compared to the IMF's and HMF's. Therefore, the peak shifts towards higher incident energies as one goes from HMF's to fragments with $A = 4$. At peripheral collisions, the multiplicity of heavy fragments is very small at all incident energies. This is due to the fact that system does not receive enough energy due to small overlap and hence cools down by emitting few nucleons/LCP's. Therefore, the peak occurs at lower incident energies at peripheral collisions. From the above study, we clearly see the onset of multifragmentation around 100 MeV/nucleon where IMF production is maximum.

In Figure 3, we display the charge yield $dN/dZ_{\rm frag}$ as a function of charge of fragments at 600 MeV/nucleon and $\hat{b} = 0$–0.75 [Figure 3(a-g)]. Interestingly, we find that, at all energies, we see a single continuous curve with negative slope in central collisions whereas it starts following a U-shape with a peak at heavier fusion products for peripheral collisions. The straight lines represents the power-law fits. The charge range used for fitting is $3 \leq Z_{\rm frag} \leq 12$. This power charge law dependence is also related to the liquid-gas phase transition, if any. All the charge yields can be nicely parameterized in terms of power law ($\propto Z_{\rm frag}^{-\varsigma}$). The

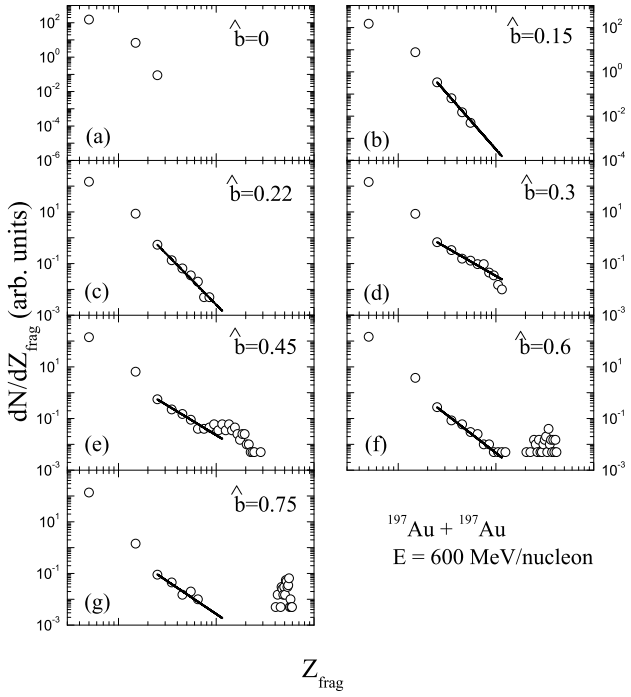

Figure 3. The charge yields curves i.e. $dN/dZ_{\rm frag}$ vs $Z_{\rm frag}$ are displayed at 600 MeV/nucleon for $\hat{b} = 0$–0.75 (a-g). The power law fits are shown by straight lines.

Table 1. The values of power factor ς obtained for different impact parameters ($\hat{b}$) and incident energies (E (MeV/nucleon)). The errors vary from 0.04 to 0.78.

E	$\hat{b}=0$	$\hat{b}=0.15$	$\hat{b}=0.22$	$\hat{b}=0.3$	$\hat{b}=0.45$	$\hat{b}=0.6$	$\hat{b}=0.75$
20	1.8	2.8	2.0	2.2	1.8	2.2	1.4
40	1.3	1.3	1.3	1.4	1.4	1.5	1.4
60	1.4	1.4	1.3	1.5	1.4	1.5	1.6
100	1.9	1.9	1.8	1.7	1.8	2.2	2.1
150	2.6	2.5	2.4	2.2	2.2	2.8	2.9
250	4.1	3.7	2.8	2.4	2.2	2.8	3.4
400	5.7	5.2	3.4	2.4	2.0	2.4	3.9
600	—	5.0	3.8	2.2	2.3	2.9	2.5
1000	—	7.1	2.9	1.8	2.3	3.4	5.2

values of ς obtained for different impact parameters and incident energies are summarized in Table 1.

The variation of ς with scaled impact parameter is shown in Figure 4 at different incident energies. It is clear from the figure, that at higher incident energies, i.e. beyond 250 MeV/nucleon, the minima in ς starts forming in $\hat{b} = 0.2$–0.4 range. For incident energies up to 150 MeV/nucleon, ς is nearly independent of colliding geometry. The range $2 < \varsigma < 3$ is the critical range of liquid-gas phase transition. Our present values of ς, do not give a clear indication about the possible liquid gas phase transition. This is due to the fact that no unique dependence of ς on impact parameter is seen. This is also predicted by one of us and collaboration [22], in a system size dependence study of ς.

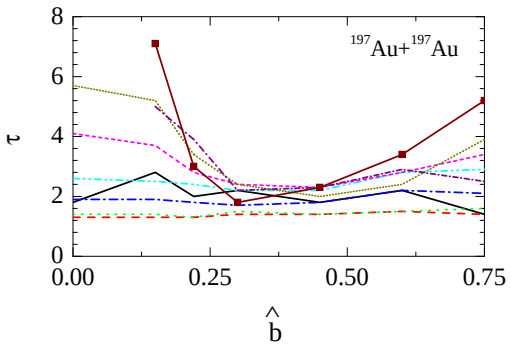

Figure 4. (Color online) The variation of power factor τ as a function of the scaled impact parameter. Lines and symbols have the same meaning as in Figure 1.

4 Summary

Using the quantum molecular dynamics model, we have carried out a systematic study of the formation of fragments with different mass ranges in the collisions of ^{197}Au+^{197}Au at incident energy between 20–1000 MeV/nucleon and at impact parameter between $\hat{b} = 0$–0.98. Our results clearly indicates the following:

(i) There is a rise and fall in the fragment production for central and semi-central collisions with an increase in the incident energy. The peak in the multiplicity occurs at higher incident energies for light mass fragments compared to heavy mass fragments. This needs experimental verification;

(ii) The IMF production as a function of impact parameter exhibits well established behavior, i.e. the multiplicity is maximum for central collisions and it decreases with the increase in impact parameter at low incident energies, whereas it has a clear rise and fall at higher incident energy;

(iii) No signal of liquid-gas phase transition are seen as no unique dependence of ς on impact parameter is seen;

(iv) We also notice that there is no rise and fall in the fragments with $A = 2$ and LCP's with change in impact parameter at all incident energies.

While the fragments with mass $A = 4$, $5 \leq A \leq 9$, $5 \leq A \leq 20$, IMF's, and HMF's show a rise and fall for $E > 400$, 250, 250, 150, and 100 MeV/nucleon. The energy of onset of multifragmentation and vaporization is found to be nearly equal to 100 MeV/nucleon and 150 MeV/nucleon, respectively. In other words, the QMD simulations of ^{197}Au+^{197}Au predict different behavior for different mass ranges than for IMF's with a change in incident energy and impact parameter.

References

[1] C.A. Ogilvie *et al.* (1991) *Phys. Rev. Lett.* **67** 1214.

[2] M.B. Tsang *et al.* (1993) *Phys. Rev. Lett.* **71** 1502.

[3] A. Schüttauf *et al.* (1996) *Nucl. Phys. A* **607** 457.

[4] D. Sisan *et al.* (2001) *Phys. Rev. C* **63** 027602;
Y.K. Vermani, R.K. Puri (2009) *J. Phys. G: Nucl. Part. Phys.* **36** 105103.

[5] J.P. Alard *et al.* (1992) *Phys. Rev. Lett.* **69** 889.

[6] G.J. Kunde *et al.* (1995) *Phys. Rev. Lett.* **74** 38.

[7] J. Hubele *et al.* (1991) *Z. Phys. A* **340** 263.

[8] M. Petrovici *et al.* (1995) *Phys. Rev. Lett.* **74** 5001;
G. Pasquali *et al.* (1995) *Nucl. Phys. A* **583** 561;
N. Bastid *et al.* (1997)*Nucl. Phys. A* **622** 573;
Andronic *et al.* (2006) *Eur. Phys. J. A* **30** 31;
W. Reisdorf *et al.* (2010) *Nucl. Phys. A* **848** 366.

[9] N. Le Neindre *et al.* (2007) *Nucl. Phys. A* **795** 47.

[10] A. Insolia *et al.* (2000) *Phys. Rev. C* **61** 044902.

[11] M. D'Agostino *et al.* (1999) *Nucl. Phys. A* **650** 329;
Y.K. Vermani, R.K. Puri (2011) *Cent. Eur. J. Phys.* **9** 621.

[12] G. Peilert *et al.* (1989) *Phys. Rev. C* **39** 1402;
H.W. Barz *et al.* (1996) *Phys. Lett. B* **382** 343;
TIAN Jun-Long *et al.* (2009) *Chin. Phys. Lett* **26** 082504;
Y.K. Vermani, R.K. Puri (2009) *Eur. Phys. Lett.* **85** 62001.

[13] R.K. Puri, S. Kumar (1999) *Pramana J. Phys.* **53** 453.

[14] P. Danielewicz (1979) *Nucl. Phys. A* **314** 465;
M.W. Curtin, H. Toki, D.K. Scott (1983) *Phys Lett. B* **123** 289.

[15] R.W. Minich *et al.* (1982) *Phys. Lett. B* **118** 458;
N.T. Porile *et al.* (1989) *Phys. Rev. C* **39** 1914.

[16] M.E. Fisher (1967) *Rep. Prog. Phys.* **30** 615; (1967) *Physics* **3** 255.

[17] M. D'Agostino *et al.* (2003) *Nucl. Phys. A* **724** 455.

[18] T. Li *et al.* (1993) *Phys. Rev. Lett.* **70** 1924;
J. Pan, S.D. Gupta (1995) *Phys. Rev. C* **51** 1384.

[19] G.F. Peaslee *et al.* (1994) *Phys. Rev. C* **49** R2271;
N.T.B. Stone *et al.* (1997) *Phys. Rev. Lett.* **78** 2084.

[20] J. Aichelin (1991) *Phys. Rep.* **202** 233;
R.K. Puri *et al.* (1994) *Nucl. Phys. A* **575** 733;
R.K. Puri, C. Hartnack, J. Aichelin (1996) *Phys. Rev. C* **54** R28;
S. Kumar, R.K. Puri (1998) *Phys. Rev. C* **58** 2858.

[21] S. Goyal, R.K. Puri (2011) *Phys. Rev. C* **83** 047601.

[22] J.K. Dhawan, R.K. Puri (2007) *Phys. Rev. C* **75** 057901.